AGU PUBLICATIONS

JGR

Journal of Geophysical Research: Space Physics

RESEARCH ARTICLE
10.1002/2014JA020907

Key Points:
- A relatively simple and computationally nonintensive model
- Flows along the magnetic field entering from opposite edges of the wake
- Plasma flow obtained here is not predicted by other models

Correspondence to:
H. Gharaee,
gharaee@ualberta.ca

Citation:
Gharaee, H., R. Rankin, R. Marchand, and J. Paral (2015), Properties of the lunar wake predicted by analytic models and hybrid-kinetic simulations, *J. Geophys. Res. Space Physics*, *120*, 3795–3803, doi:10.1002/2014JA020907.

Received 5 DEC 2014
Accepted 22 APR 2015
Accepted article online 27 APR 2015
Published online 29 May 2015

Properties of the lunar wake predicted by analytic models and hybrid-kinetic simulations

Hossna Gharaee[1], Robert Rankin[1], Richard Marchand[1], and Jan Paral[2]

[1]Department of Physics, University of Alberta, Edmonton, Alberta, Canada, [2]High Altitude Observatory, NCAR, Boulder, Colorado, USA

Abstract An approximate model derived by Hutchinson (2008a), describing the interaction between the solar wind and the Moon, is applied to describe plasma in the lunar wake. The model accounts for plasma entering the wake region from two tangent points around the Moon. Cylindrical geometry is assumed, along with a strong constant magnetic field, and fixed transverse velocity and temperature. Under these approximations two angle-dependent equations for fluid flow are obtained, which can be solved using the method of characteristics to provide the density inside the wake region. It is demonstrated that the model valid under these assumptions provides excellent agreement with observations from the ARTEMIS mission and with large-scale hybrid-kinetic plasma simulations. The model provides a practical alternative to kinetic simulations and is generally useful for determining properties of the lunar wake under different solar wind conditions. It will be useful as well for predicting properties of the plasma environment around unmagnetized bodies that have not yet been visited by spacecraft.

1. Introduction

Various models have been used to simulate the interaction between Earth's Moon and the solar wind. *Harnett and Winglee* [2002] applied a 2.5-D MHD model to simulate the solar wind interaction with localized magnetic fields at the surface of the Moon and found structures similar to Earth's magnetopause and bow shock near magnetic field anomalies, with positions and shapes varying with solar wind conditions. ARTEMIS data support the outward expansion of the lunar wake in the near-moon region at magnetosonic velocities as is predicted by MHD models *Zhang et al.* [2012]. More recently *Xie et al.* [2013] used the Space Weather Modeling Framework [*Toth et al.*, 2012] to study asymmetries in the lunar wake associated with different orientations of the solar wind magnetic field and plasma flow velocity.

Hybrid models in which ions are treated kinetically, and electrons as a fluid, have been applied to study macroscopic and fine-scale kinetic aspects of lunar wake dynamics. For example, 2-D hybrid-kinetic models have revealed that the downstream region ($28R_L < x < 40R_L$) of the lunar wake is dominated by low-frequency electromagnetic turbulence [*Travnicek et al.*, 2005]. *Kallio* [2005] presented the first 3-D hybrid simulation of the solar wind-Moon interaction and showed that a long tail ($> 10R_L$) of depleted plasma density forms in the nightside, along with an enhancement of the magnetic field in the wake boundary and a decreased field in the center of the wake. *Wang et al.* [2011] used a 3-D hybrid code to study electromagnetic disturbances in the solar wind and showed that the magnetic field was enhanced by a factor of about 1.4 in the middle of the lunar wake, with depletions at the two sides due to the lunar absorption effect. A similar approach used by *Holmstrom et al.* [2012] predicts the occurrence of kinks in the magnetic field at the wake boundary.

Farrell et al. [1998] analyzed kinetic features of the lunar wake using a one-dimensional electrostatic particle-in-cell (PIC) code. The PIC model was able to reproduce wakeward directed ion beams generated by ambipolar electric fields formed at the wake edge, consistent with Wind observations of counter-streaming ion beams in the wake region. The electric field structure around the Moon has also been studied using 2-D electromagnetic PIC simulation. The results of one such study [*Kimura and Nakagawa*, 2008] predict the formation of an intense electric field at the terminator region where the electric field produced by the negatively charged lunar surface and the ambipolar electric field at the wake boundary are in the same direction.

In contrast with the complex computational approaches mentioned above, Hutchinson developed a relatively simple and fast analytic approach capable of reproducing many features of plasma dynamics at the edge of the lunar wake [*Hutchinson*, 2008a, 2008b, 2013]. The approach rests on the assumptions that (i) the solar

wind is strongly magnetized, (ii) plasma can be treated as a quasi-neutral isothermal fluid, (iii) the ion polarization drift can be neglected, and (iv) the magnetic field is constant and uniform everywhere in space. These assumptions lead to a set of two coupled equations for the ion density and plasma Mach number, which can be solved by the method of characteristics. Hutchinson modeled the density and plasma flow velocity near the edge of the wake for cases in which the Interplanetary Magnetic Field (IMF) is perpendicular to the flow. The main purpose of this paper is to apply Hutchinson's theory to cover the entire wake region by accounting for the fact that plasma enters the wake by streaming along magnetic field lines from above and below the wake edges.

As explained below, this simplified model readily leads to estimates of counterstreaming plasma flows parallel to magnetic field lines in the wake; flows that are not easily obtained from standard MHD models and which are difficult to extract from kinetic simulations because of the relatively low density of wake particles. In section 2 of this paper, Hutchinson's lunar wake model is reviewed and equations are derived that incorporate two ion fluids streaming into the wake. In section 3 comparisons are made with simulation results from a 2-D hybrid model developed by *Paral and Rankin* [2013] and with ARTEMIS satellite observations [*Angelopoulos*, 2011]. Finally, a summary and concluding remarks are presented in section 4.

2. Methodology

The two-dimensional fluid approach proposed by Hutchinson to describe the edge of the lunar wake, and the two-dimensional hybrid code used in the paper have been described in earlier publications [*Hutchinson*, 2008a, 2008b, 2013; *Paral and Rankin*, 2013]. These approaches are briefly summarized, while Hutchinson's approach is modified to describe the cross section of the wake.

2.1. Plasma Entry to the Lunar Wake

The basic assumptions in Hutchinson's model are as follows: (1) particle gyro-radii are much smaller than any macroscopic scale length in the problem, (2) plasma is quasi-neutral, (3) ions and electrons can be described as single isothermal fluids, (4) the solar wind magnetic field is constant and uniform, (5) electron inertia and the ion polarization drift are negligible, and (6) the ion velocity component perpendicular to the magnetic field is constant and uniform.

From these assumptions, and using the electron parallel momentum equation, one finds the familiar adiabatic relation between the electric potential $\nabla_\parallel \phi$ and parallel pressure gradients

$$E_\parallel = -\nabla_\parallel \phi = -\frac{1}{en}\nabla_\parallel p_e = -\frac{T_e}{e}\nabla_\parallel \ln(n), \tag{1}$$

where the subscript e refers to electrons, and use is made of the ideal gas law $p_e = nT_e$. It can then be shown that the ion continuity and momentum equations, combined with the electron momentum equation, reduce to the following two coupled equations for the ion density n and Mach number M:

$$\vec{M}\cdot\nabla \ln(n) + \nabla_\parallel M_\parallel = 0, \tag{2}$$

and

$$\vec{M}\cdot\nabla M_\parallel + \nabla_\parallel \ln(n) = 0, \tag{3}$$

where, $\vec{M} = \vec{v}/c_s$, and $c_s^2 = (ZT_e + \gamma T_i)/m$ is the square of the ion acoustic speed. In this expression, m, Z, T_e, and T_i are, respectively, the ion mass and charge number, the electron and ion temperatures, and the adiabatic index $\gamma = 5/3$. By adding and subtracting these equations, it follows that

$$(\vec{M}\cdot\nabla + \nabla_\parallel)(\ln(n) + M_\parallel) = 0, \tag{4}$$

and

$$(\vec{M}\cdot\nabla - \nabla_\parallel)(\ln(n) - M_\parallel) = 0, \tag{5}$$

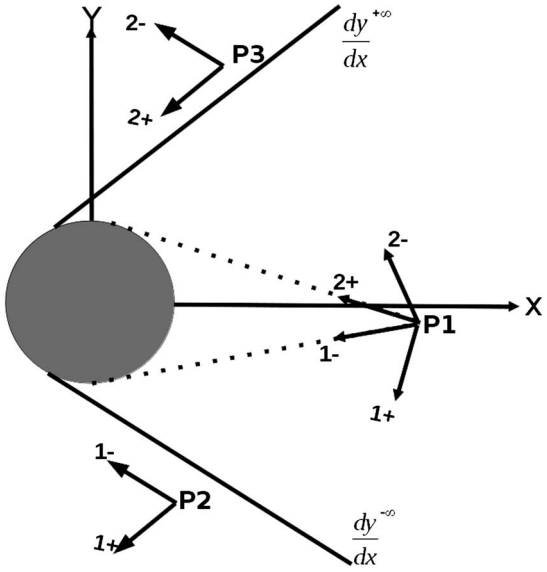

Figure 1. Illustration of the unperturbed solar wind and lunar wake regions. Points P2 and P3 are located, respectively, below and above the wake in the unperturbed region of the solar wind, while P1 is in the wake. Vectors identified with + and − are pointing in the $-x$ direction along the positive and negative characteristics, respectively. The labels 1 and 2 on these vectors refer to plasma below and above the wake in the unperturbed plasma, or entering the wake from below and above the wake boundaries, respectively. The two lines labeled $\frac{dy}{dx}|^{\pm\infty}$ show the boundary between the unperturbed solar wind and the wake. Their slope is that of the + and − upstream characteristic, and they are tangent to the Moon above and below the lunar disk, respectively.

are two decoupled equations for the two independent variables $\ln(n) \pm M_{\parallel}$ that can be solved straightforwardly using the method of characteristics. In particular, it follows from equations (4) and (5) that $\ln(n) \pm M_{\parallel}$ are constant, respectively, along the characteristics defined by the equations

$$\left.\frac{dx}{ds}\right|^{\pm} = M_x \pm \frac{B_x}{B} \tag{6}$$

and

$$\left.\frac{dy}{ds}\right|^{\pm} = M_y \pm \frac{B_y}{B}, \tag{7}$$

where ds is the infinitesimal element of length along the characteristics, and the $\pm$ superscripts refer to positive and negative characteristics, respectively. In the upstream solar wind $\pm$ characteristics are then straight lines with slopes which are derived by taking the ratio of the right-hand sides of equation (7) to equation (6).

By using this formalism, *Hutchinson* [2013] was able to model the edge of the lunar wake. Referring to Figure 1, and assuming that plasma entering the wake is coming predominantly from one side of the Moon, say from below, he argued that in the wake the parallel Mach number must be such that the negative characteristic is tangent to the Moon from below. This leads to the following equation for the plasma density associated with parallel flow coming from below:

$$n = n_0 \exp\left(-|M_{\parallel} - M_{0\parallel}|\right), \tag{8}$$

where $M_{0\parallel}$ is the upstream plasma parallel velocity. We now apply this approach to the full width of the wake by considering the plasma flow entering the wake from both below and above the wake as shown in Figure 1.

Compared with Hutchinson's original analysis in which only one ion fluid was considered near the wake edge, we need to account for two ion fluids coming from either side of the Moon cross section. As we shall see later, these counterstreaming ion flows are important in determining properties of the wake region plasma. We account for the two ion fluids by labeling them with subscripts 1 and 2, corresponding to plasma entering from below and above, respectively, as discussed by *Hutchinson* [2012]. Each ion fluid is characterized by a density $n_{1,2}$ and a parallel Mach number $M_{1,2\parallel}$, and is governed by two characteristic equations similar to equations (4) and (5). The main difference here comes from the relation between the parallel electric field and the electron pressure gradient. Making use of the quasi-neutrality assumption and accounting for the two ion fluids, equation (1) now reads

$$\nabla_{\parallel}\phi = \frac{T_e}{e}\left(\frac{n_1}{n_1+n_2}\nabla_{\parallel}\ln(n_1) + \frac{n_2}{n_1+n_2}\nabla_{\parallel}\ln(n_2)\right). \tag{9}$$

Then, following the same steps as outlined above for Hutchinson's model, one finds

$$(\vec{M}_1 \cdot \nabla + \nabla_{\parallel})(\ln(n_1) + M_{1\parallel}) = \frac{ZT_e}{T_i + ZT_e}\frac{n_2}{n_1+n_2}\nabla_{\parallel}\left(\ln(n_1) - \ln(n_2)\right), \tag{10}$$

$$(\vec{M}_1 \cdot \nabla - \nabla_\parallel)(\ln(n_1) - M_{1\parallel}) = -\frac{ZT_e}{T_i + ZT_e}\frac{n_2}{n_1 + n_2}\nabla_\parallel\left(\ln(n_1) - \ln(n_2)\right), \tag{11}$$

$$(\vec{M}_2 \cdot \nabla + \nabla_\parallel)(\ln(n_2) + M_{2\parallel}) = -\frac{ZT_e}{T_i + ZT_e}\frac{n_1}{n_1 + n_2}\nabla_\parallel\left(\ln(n_1) - \ln(n_2)\right), \tag{12}$$

and

$$(\vec{M}_2 \cdot \nabla - \nabla_\parallel)(\ln(n_2) - M_{2\parallel}) = \frac{ZT_e}{T_i + ZT_e}\frac{n_1}{n_1 + n_2}\nabla_\parallel\left(\ln(n_1) - \ln(n_2)\right). \tag{13}$$

This system of four coupled inhomogeneous equations is more difficult to solve in general than the two equations derived by Hutchinson for a single ion fluid. The reason is that owing to the nonzero right-hand-sides, the dependent variables are not exactly constant along characteristics. Consequently, in contrast to the single ion fluid case, the characteristics are not exactly straight lines. The solutions could be obtained iteratively using the method of characteristics or by discretization of equations (10) to (13) using finite differences and specifying appropriate boundary conditions. In the following, equations (10) to (13) are solved approximately simply by neglecting the right-hand sides. This means that the two ion fluids streaming from above and below the wake do not affect one another. In this case, the system of four homogeneous equations reduces to a set of two uncoupled homogeneous equations that can be solved as in Hutchinson's original analysis. The resulting densities n_1 entering below and n_2 entering from above are then added to give the total plasma wake density.

The approximations we have made above are further validated by the good agreement with results obtained using another model (which does not make these approximations) and observations in the sections 3.1 and 3.2. In order to explain the solution procedure, it is useful to write explicit expressions for the characteristics. Assuming an angle α between the magnetic field and the solar wind flow velocity, the magnetic field, the Mach number vector, and the parallel gradient are written as

$$\vec{B} = B(\cos(\alpha)\hat{x} + \sin(\alpha)\hat{y}), \tag{14}$$

$$\vec{M} = [M_\perp \sin(\alpha) + M_\parallel \cos(\alpha)]\hat{x} + [-M_\perp \cos(\alpha) + M_\parallel \sin(\alpha)]\hat{y}, \tag{15}$$

and

$$\nabla_\parallel = (\cos(\alpha)\partial/\partial x)\hat{x} + (\sin(\alpha)\partial/\partial y)\hat{y}, \tag{16}$$

where, consistent with Hutchinson's model, $M_\perp$ is assumed to be constant. Omitting subscripts 1 and 2 for brevity, the homogeneous approximation of equations (10) to (13) then becomes

$$\left[(M_\perp \sin(\alpha) + M_\parallel \cos(\alpha) + \cos(\alpha))\frac{\partial}{\partial x} + (-M_\perp \cos(\alpha) + M_\parallel \sin(\alpha) + \sin(\alpha))\frac{\partial}{\partial y}\right][\ln(n) + M_\parallel] = 0, \tag{17}$$

$$\left[(M_\perp \sin(\alpha) + M_\parallel \cos(\alpha) - \cos(\alpha))\frac{\partial}{\partial x} + (-M_\perp \cos(\alpha) + M_\parallel \sin(\alpha) - \sin(\alpha))\frac{\partial}{\partial y}\right][\ln(n) - M_\parallel] = 0. \tag{18}$$

The equations for the two characteristics are then

$$\left.\frac{dy}{dx}\right|^{\pm} = \frac{\pm\sin(\alpha) - M_\perp \cos(\alpha) + M_\parallel \sin(\alpha)}{\pm\cos(\alpha) + M_\perp \sin(\alpha) + M_\parallel \cos(\alpha)}. \tag{19}$$

In the upstream region ($x \to -\infty$) where plasma is unperturbed, the Mach vector $\vec{M}_0$ is purely along x, which leads to

$$M_{0\perp} = M_0 \sin(\alpha), \tag{20}$$

Table 1. Main Similarities and Differences Between the Analytic and Hybrid Models

	Analytic	Hybrid
Similarities	2-D cylindrical	
	Isothermal fluid electrons	
Differences	Magnetized fluid ions	Kinetic ions
	Stationary	Time dependent
	Uniform and constant $\vec{B}$	Solves for $\vec{E}$ and $\vec{B}$
	$M_\perp$ constant	$M_\perp$ variable

$$M_{0\parallel} = M_0 \cos(\alpha). \tag{21}$$

From this and equation (19), it follows that the equations for the upstream characteristics are

$$\left.\frac{dy}{dx}\right|_0^{\pm} = \frac{\pm \sin(\alpha)}{\pm \cos(\alpha) + M_0}. \tag{22}$$

In the following we limit our attention to the special case where the magnetic field is perpendicular to the upstream flow velocity, that is, to $\alpha = 90°$. From equation (22), it follows that the $\pm$ characteristics are then straight lines with slopes $\pm 1/M_0$.

The equations for the upstream characteristics can be used to distinguish between the unperturbed solar wind and the wake regions. By assumption, the upstream solar wind is unperturbed as $x \to -\infty$. Owing to the constancy of $\ln(n) \pm M_\parallel$ along the $\pm$ characteristics, it follows that the incoming solar wind at any point P in Figure 1 will be unaffected, that is, $n = n_0$ and $M_\parallel = M_0$ if and only if P can be moved continuously toward $x \to -\infty$ in such a way that none of the unperturbed characteristics given in equation (22) intersect the Moon. Conversely, the wake is the region where points cannot be moved continuously toward $x \to -\infty$ without at least one of the unperturbed characteristics intersecting the Moon. From this, it follows that the wake region is delimited by the positive and negative characteristic tangent, respectively, above and below the disk of the Moon, as illustrated in Figure 1. The question then is how does one compute densities n_1 and n_2 in the wake region? This is done with a straightforward extension of Hutchinson's approach for the edge of the wake, in which a single ion density is considered. Recalling that n_1 and n_2 are the ion density entering the wake, respectively, from below and above, and referring to Figure 1, these densities are obtained from

$$n_{1,2} = n_0 \exp(-|M_{1,2\parallel} - M_{0\parallel}|) \tag{23}$$

where $M_{1\parallel}$ is set in order for the negative characteristic to be tangent below the lunar disk for n_1, and similarly, $M_{2\parallel}$ is set in order for the positive characteristic to be tangent above for n_2.

2.2. Hybrid Code

The 2-D hybrid-kinetic electromagnetic model, previously used by *Paral and Rankin* [2013] to model the solar wind interaction with planet Mercury, is employed in order to assess the validity of the analytic model of the lunar wake. This model ignores electron kinetic effects but correctly accounts for ion gyroradius effects that are important for small-scale structures like discontinuities formed in the lunar wake. Electrons are treated as a massless, charge-neutralizing fluid, which prohibits parallel electric fields from forming, while ions are considered as particles. In addition, the low-frequency magnetostatic (Darwin) approximation is made by ignoring the displacement current in Maxwell's equations. This leads to a set of equations which describe the temporal and spatial evolution of the electromagnetic fields and the plasma [*Paral*, 2013; *Matthews*, 1994]. A summary of the main similarities and differences between the analytic and the hybrid models is given in Table 1.

2.3. Mapping a 2-D Wake Into 3-D

A procedure is needed to map 2-D results obtained from the analytic model into an actual 3-D lunar wake. The procedure makes use of the fact that the characteristics, the Mach vector, and the magnetic field, all lie in a single plane. The problem of solving for $M_\parallel$ and n in 3-D then reduces to a 2-D problem in the plane containing $\vec{B}$ and $\vec{v}$. Thus, the procedure outlined in section 2.1 above can be applied without any change, except for the cross section of the Moon, which must now be taken as the intersection of the 3-D Moon with that plane. Furthermore, it can be seen that in the simplified analytic MHD description of the wake and solar wind, the ratio n/n_0 and $M_\parallel$, only depend on the relative position $\vec{r}/R_c$ in the $\vec{B}$ - $\vec{v}$ plane, where R_c is the radius of this cross section. In the particular case considered in the next section, where $\vec{v}_0$ is along x and $\vec{B} \parallel \hat{y}$, the 2-D plane of interest is simply the $x-y$ plane and the radius of the Moon cross section in the $x-y$ plane containing the satellite is given by $R_c = \sqrt{R_M^2 - y_{SC}^2}$, where R_M is the lunar radius and y_{SC} is the y coordinate of the spacecraft. It

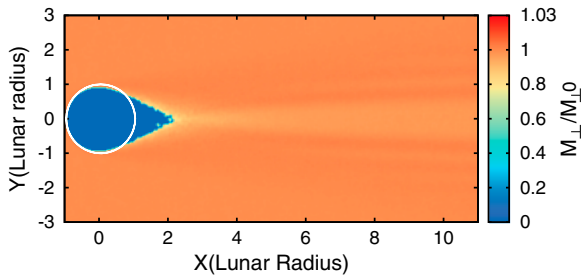

Figure 2. Ratio of the perpendicular Mach number to its upstream value $\frac{M_\perp}{M_{0\perp}}$ in the hybrid simulation domain.

should be noted that in this two-dimensional approximation, no plasma flow in the z direction perpendicular to the $\vec{B}-\vec{v}$ plane is taken into account.

3. Results

Now we compare results obtained from the 2-D analytic model with those of the hybrid model and with ARTEMIS observations. This serves to assess the validity of the assumptions made in the analytic model and its accuracy in describing the main features of the lunar wake. One constraint is introduced into the hybrid model: the time evolution of the solar wind magnetic field is artificially turned off to be consistent with the assumption made in the analytic model. We note that although several models have proposed to simulate convection and diffusion of the IMF through the Moon, these models are not ideal for comparison because they make ad hoc assumptions that cause perturbations in $\vec{B}$ to depend on their specific implementation. This is primarily a result of the low-density plasma inside the wake; for models to be numerically stable, particles are artificially injected into the wake from the nightside of the Moon. A more physical assumption for assuming that $\vec{B}$ is constant is that because of the low conductivity of the Moon, the IMF penetrates more or less unimpeded. The constant magnetic field approximation is also supported by the relatively small variations in $\vec{B}$ observed with ARTEMIS [*Wiehle et al.*, 2011]. The increase in $\vec{B}$ within the wake is not accounted for in the analytic formalism, but this is offset by the specification of other wake properties that it provides. After comparing the results of the analytic and hybrid models, we proceed to compare them with in situ ARTEMIS spacecraft wake density measurements. The section is then concluded with a discussion of the two parallel Mach numbers $M_{1,2\|}$ introduced in the previous section.

3.1. Results Obtained From the Analytic and the Hybrid Models

In the 2-D hybrid code and analytic models the solar wind flow is assumed to be in the $+x$ direction, and the solar wind magnetic field $\vec{B}_{\rm IMF}$ is in the $+y$ direction ($\alpha = 90°$) with a magnitude of 6 nT [*Tao et al.*, 2012]. The solar wind speed is 295.6 km/s [*Wiehle et al.*, 2011], the background density is $n_{\rm sw} = 3.14$ cm^{-3}, the electron and ion temperatures are $T_e \simeq 14.3$ eV ($\beta_e \simeq 0.5$), and $T_{\rm i} \simeq 5.7$ eV ($\beta_i \simeq 0.2$). These parameters are the same as those considered in the comparison with ARTEMIS measurements discussed in section 3.2. The dimensions of the simulation box used in the hybrid model is (400×400) $(c/\omega_{\rm p,i0})$ where c is the speed of light, $\omega_{\rm p,i0}$ is the proton plasma frequency in the ambient solar wind, and $c/\omega_{\rm p,i0}$ is the inertial length of the solar wind protons, i.e., $\sim$ 129.58 km. In the hybrid code the grid cell size and time step are set to be $(0.5 \times 0.5)(c/\omega_{\rm p,i0})$ and $\Delta t = 0.006\ \Omega_{i0}^{-1}$, respectively, where $\Omega_{\rm i0} \sim 0.38$ s^{-1} is the proton gyrofrequency in the solar wind. With these parameters, the simulation domain used in the hybrid simulations extends over $\pm 11\ R_{\rm M}$ in X and $\pm 5\ R_{\rm M}$ in Y, where $R_{\rm M} \sim 1737$ km. They correspond to those from the first flyby of ARTEMIS P1 through the lunar wake. Specifically, with the parameters given above, the sound speed is $c_{\rm s} \sim 48.8$ km/s and the corresponding upstream Mach number is $M_\perp \simeq 6$ and $M_\| = 0$. We recall that in the hybrid code the perpendicular velocity is not assumed to be constant while it is in the analytic model.

As a first comparison, Figures 2 and 3 show the perpendicular Mach number, normalized to its upstream value and the density obtained from the hybrid model. In contrast to the assumption of constant perpendicular velocity made in the analytic model, Figure 2 shows small variations in $v_\perp$ in the wake region. From Figure 3, however, these variations are seen to occur in the very low density regions, where statistical errors in $M_\perp$ are large. In regions where the density is significant (say, above 2.8% of the background density), $M_\perp$ is found to be constant within ~9%. In those regions, the maximum relative difference is of the order 9%, which supports the assumption made in the analytic model

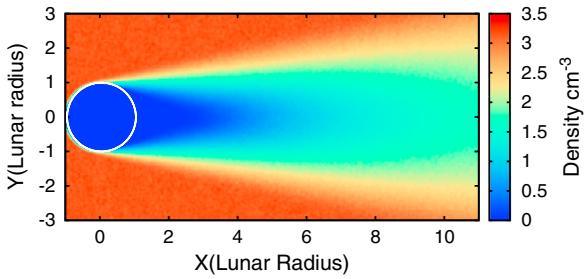

Figure 3. Density of the plasma in the hybrid simulation domain.

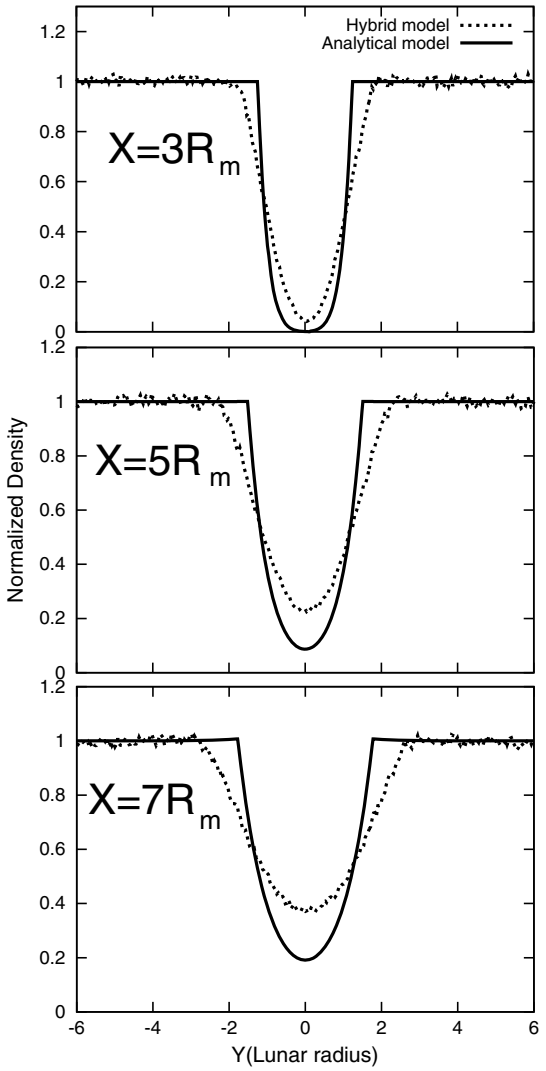

Figure 4. Comparison between the normalized ion density obtained with the hybrid code (dotted line) and analytic model (solid line) along Y at different cuts in X. From top to bottom, $X = 3R_m$, $X = 5R_m$, and $X = 7R_m$. Densities are normalized to the upstream solar wind density in both models.

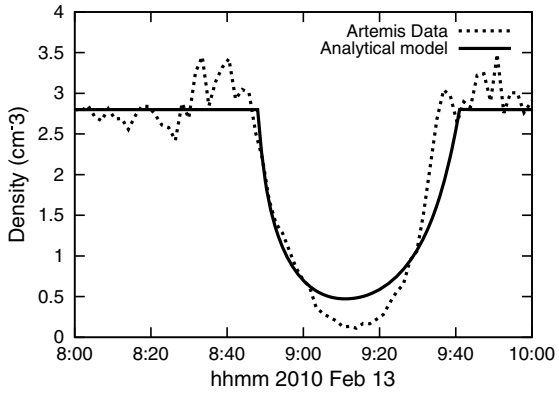

Figure 5. Comparison of ARTEMIS data (dotted line) and the analytic model ion density.

that $M_\perp$ is approximately constant. A second comparison is between the density computed with the two approaches. Figure 4 plots normalized densities obtained from the hybrid and analytic models as a function of the vertical coordinate Y, at selected values of X in the wake region. In both cases, the density is found to be minimum at the center of the wake and increases as expected away from the Moon. Differences in the density profiles obtained with the two models are visible from this figure. Qualitatively, the density profile obtained from the hybrid model is narrower near the minimum and broader in the wake edge region than the density obtained analytically. In the analytic model the magnetic field is assumed to be constant. This assumption is also applied to the hybrid code. As a consequence, fast mode MHD waves are omitted from the analysis. Another difference is that the analytic model predicts smooth density profiles, while the ones obtained with the hybrid code show significant levels of short-scale variations, probably associated with waves and turbulence excited in the solar wind-Moon interaction. Quantitatively, the minimum density obtained analytically is lower than that in the hybrid model. These differences are relatively small and do not exceed 17% of the upstream density, from which we conclude that both models predict density profiles that are in good agreement.

3.2. Comparison Between Theory and Observations

We now consider a comparison between the density estimated analytically along the trajectory of the P1 spacecraft of the ARTEMIS mission during its first flyby through the lunar wake. In this first flyby, the Moon was located outside the magnetosphere, between the Earth and the Sun, so the solar wind was not perturbed by the presence of Earth's magnetosphere. The satellite went through the wake at a distance of $\sim$3.5 R_M from the Moon center downstream. This event occurred on 13 February 2010 between 08:53 and 09:29 UT [*Wiehle et al.*, 2011; *Tao et al.*, 2012]. The input parameters used in the analytic model ($M_\perp \simeq 6$ and $\alpha = 90°$) are the same as those used in the comparison with the hybrid model presented in section 3.1. Figure 5 shows both the analytically computed (solid) and measured (dots) densities as a function of time. The density obtained analytically is seen to be in good agreement with measured values. Quantitatively, the two densities agree within $\simeq$12%

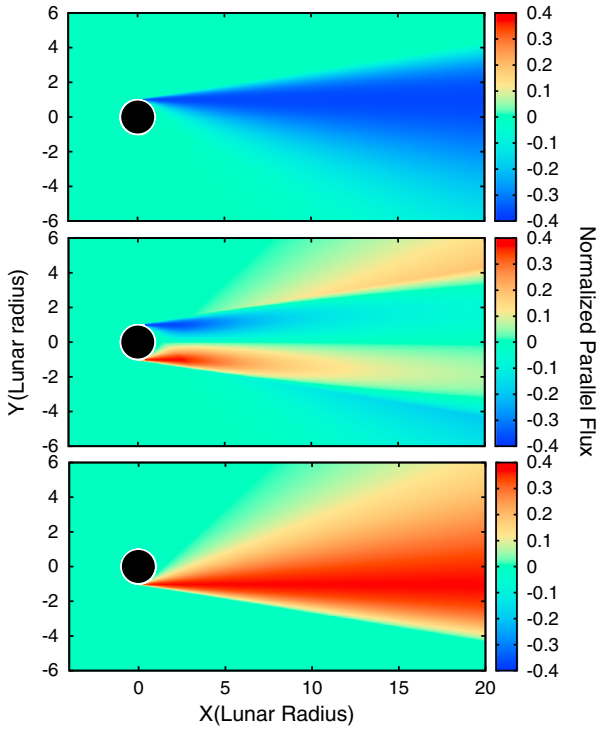

Figure 6. Normalized plasma parallel fluxes along the magnetic field are obtained from the analytic model. Plasma fluxes entering the wake from (top) above and (bottom) below are shown. (middle) The net normalized parallel flux ($\Gamma = \Gamma_{1\|} + \Gamma_{2\|}$). Normalized fluxes are defined as $\Gamma_{1,2\|} = (n_{1,2}M_{1,2\|})/n_{sw0}$.

almost everywhere, the exception being in a narrow range at the wake edge where the discrepancy does not exceed ≃25%. Qualitatively, the shapes of the wakes are similar. The depth of the wake from ARTEMIS data is ∼3.9% of the background plasma density, while that obtained from the analytic model is higher ∼16.2%. Another difference to be noted is the presence of short-scale variations in the ARTEMIS data, while the analytic density profile is smooth. Moving toward the Moon from the nightside, the observed density depletion is smaller than the analytic model predicts at large distances from the Moon. However, the observed and predicted density are nearly equal within ∼3.5 R_M.

3.3. Parallel Plasma Flow

As well as density, the analytic model provides the parallel flow velocity of ions entering the wake. A result of the analytic model, which is not obtained from single fluid numerical simulation models, is an explicit expression for the parallel flow velocity of ions entering the wake from below and above. The pressure gradient at the lower edge of the wake drives parallel plasma flow upward, and similarly, the pressure gradient at the upper edge drives parallel flow downward into the wake. This is illustrated in Figure 6, which shows the normalized parallel ion flux $\Gamma_{1,2\|} = (n_{1,2}M_{1,2\|})/n_{sw0}$, where n_{sw0} is the upstream solar wind density and the net normalized flux $\Gamma = \Gamma_{1\|} + \Gamma_{2\|}$. Figure 6 (middle) shows the approximate net flux which would be obtained from a fluid simulation: negative and positive parallel flow, above and below the x axis, corresponds to plasma entering the wake from above and below, respectively. The net ion parallel flow at the center of the wake (at $y = 0$) vanishes by symmetry, but the fact that it is associated with two counterstreaming flows would be missing from single fluid models. The study of the consequences of these two counterstreaming parallel flows is beyond the scope of this paper, but it is worth noting that these constitute a source of free energy that could lead to dynamic processes such as wave generation or turbulence.

4. Conclusion

In this paper we have extended and made use of an analytic model of the lunar wake first proposed by *Hutchinson* [2013] to model the edge of the lunar wake. Ion density profiles obtained with this model have been compared with those from a 2-D hybrid model developed by *Paral and Rankin* [2013], and generally good agreement has been found. We have also compared the results of the analytic model with data from an ARTEMIS P1 flyby. The good qualitative and quantitative agreement between the two indicates that despite its simplicity the analytic model is capable of capturing much of the physics at play in the formation of the lunar wake. In particular, the assumption made in the analytic model that the perpendicular plasma velocity is constant and uniform, has been verified within ∼9% in regions where the plasma density is ∼2.8% of the upstream solar wind density or more. This is of interest because it suggests that some key parameters of the wake, such as the density and the plasma flow parallel to the magnetic field ($M_{\|}$ in our equations), can be well approximated with a relatively simple and computationally nonintensive model. The 2-D analytic model presented here can also be used to estimate quantities that are not predicted by more complex two- or three-dimensional MHD fluid models and that are not readily obtained from kinetic simulation. An example is counterstreaming flows along the magnetic field associated with plasma entering from opposite (along $\vec{B}$) edges of the wake. In a single-fluid description of plasma, including multifluid models, only one density

and flow velocity is considered for each species, whether that species is considered upstream or downstream of an obstacle. Thus, an important source of free energy and possible source of instability and turbulence in the wake is missed in these approaches. The presence of two or more counterstreaming plasma flows is of course included in both hybrid and full PIC simulations. The parameterization of these flows, however, is not straightforward, as it requires the calculation of higher moments of the distribution function or a discretization of the distribution function from counting particles in many velocity bins taken from a small volume in configuration space. While straightforward in principle, either approach would require a small sampling box with a very large number of particles in order to reduce statistical errors.

Acknowledgments

This work was partially supported by grants from the Canadian Space Agency and the Natural Sciences and Engineering Research Council of Canada (NSERC). The simulations also benefited from access to the Westgrid Compute Canada facilities. The ARTEMIS data for this paper are available at NASA's Space Physics Data Facility (SPDF) (http://spdf.gsfc.nasa.gov/). Hossna Gharaee extends thanks to THEMIS software manager Jim Lewis and graduate student Chengrui Wang for their help on using ARTEMIS satellite data. Hossna Gharaee would like to thank Michael Wise for his help on producing figures of this paper. Jan Paral would like to acknowledge the hospitality and support of the National Center for Atmospheric Research which is supported by the National Science Foundation.

Yuming Wang thanks the reviewers for their assistance in evaluating this paper.

References

Angelopoulos, V. (2011), The ARTEMIS mission, *Space Sci. Rev.*, *165*(1–4), 3–25.

Farrell, W., M. Kaiser, J. Steinberg, and S. Bale (1998), A simple simulation of a plasma void: Applications to Wind observations of the lunar wake, *J. Geophys. Res.*, *103*(A10), 23,653–23,660.

Harnett, E., and R. Winglee (2002), 2.5D particle and MHD simulations of mini-magnetospheres at the Moon, *J. Geophys. Res.*, *107*(A12), 1421, doi:10.1029/2002JA009241.

Holmstrom, M., S. Fatemi, Y. Futaana, and H. Nilsson (2012), The interaction between the Moon and the solar wind, *Earth Planets Space*, *64*(2), 237–245.

Hutchinson, I. (2008a), Oblique ion collection in the drift approximation: How magnetized Mach probes really work, *Phys. Plasmas*, *15*(12), 123503.

Hutchinson, I. (2008b), Ion collection by oblique surfaces of an object in a transversely flowing strongly magnetized plasma, *Phys. Rev. Lett.*, *101*(3), 035004, doi:10.1103/PhysRevLett.101.035004.

Hutchinson, I. (2012), Electron velocity distribution instability in magnetized plasma wakes and artificial electron mass, *J. Geophys. Res.*, *117*, A03101, doi:10.1029/2011JA017119.

Hutchinson, I. (2013), Near-lunar proton velocity distribution explained by electrostatic acceleration, *J. Geophys. Res. Space Physics*, *118*, 1825–1827, doi:10.1002/jgra.50277.

Kallio, E. (2005), Formation of the lunar wake in quasi-neutral hybrid model, *Geophys. Res. Lett.*, *32*, L06107, doi:10.1029/2004GL021989.

Kimura, S., and T. Nakagawa (2008), Electromagnetic full particle simulation of the electric field structure around the Moon and the lunar wake, *Earth Planets Space*, *60*(6), 591–599.

Matthews, A. (1994), Current advance method and cyclic leapfrog for 2D multispecies hybrid plasma simulations, *J. Comput. Phys.*, *112*, 102–116.

Paral, J. (2013), Hybrid-kinetic modelling of space plasma with application to Mercury, PhD thesis, Univ. of Alberta, Alberta, Canada.

Paral, J., and R. Rankin (2013), Dawn-dusk asymmetry in the Kelvin-Helmholtz instability at Mercury, *Nat. Commun.*, *4*, 1645, doi:10.1038/ncomms2676.

Tao, J., et al. (2012), Kinetic instabilities in the lunar wake: ARTEMIS observations, *J. Geophys. Res.*, *117*, A03106, doi:10.1029/2011JA017364.

Toth, G., et al. (2012), Adaptive numerical algorithms in space weather modeling, *J. Comput. Phys.*, *231*(3), 870–903.

Travnicek, P., P. Hellinger, D. Schriver, and S. Bale (2005), Structure of the lunar wake: Two-dimensional global hybrid simulations, *Geophys. Res. Lett.*, *32*, L06102, doi:10.1029/2004GL022243.

Wang, Y.-C., J. Muller, W.-H. Ip, and U. Motschmann (2011), A 3D hybrid simulation study of the electromagnetic field distributions in the lunar wake, *Icarus*, *216*(2), 415–425.

Wiehle, S., et al. (2011), First lunar wake passage of ARTEMIS: Discrimination of wake effects and solar wind fluctuations by 3D hybrid simulations, *Planet. Space Sci.*, *59*(8), 661–671.

Xie, L., L. Lei, Z. YiTeng, and D. Zeeuw (2013), Three-dimensional MHD simulation of the lunar wake, *Sci. China Earth Sci.*, *56*(2), 330–338.

Zhang, H., et al. (2012), Outward expansion of the lunar wake: Artemis observations, *Geophys. Res. Lett.*, *39*, L18104, doi:10.1029/2012GL052839.